Supplementary Materials for

An ultrasound-scanning *in vivo* light source

Table of Contents:

Supplementary Text

Estimation of optical power from circulating mechanoluminescent nanotransducers (MLNTs)

To quantify the optical power of mechanoluminescence emission, we employed a photodiode to measure the power of the ultrasound-mediated light source in the artificial circulatory system (**Supplementary Fig. 4a**). The mechanoluminescence emission induced by focused ultrasound (FUS) is treated as a cylindrical light source (**Supplementary Fig. 4b**), with its diameter determined by the emission spot size in the image and height determined by the tubing diameter (since the axial point spread function of the ultrasound focus is longer than the tubing diameter).

To minimize background noise, the measured power attributed to mechanoluminescence is calculated by subtracting the baseline power ($P_{baseline}$) from the peak power (P_{peak}) during FUS pulses. An additional correction factor F accounts for the contribution of persistent luminescence after the cessation of ultrasound stimulation. The total emitted power from the upper surface of the cylindrical light source (P_{total}) is estimated using the equation below:

$$P_{total} = \frac{(P_{peak} - P_{baseline}) 2\pi D^2 F}{A\,T} \quad (1)$$

where P_{peak}, $P_{baseline}$, and F are defined above; D is the distance between the inner surface of the tubing and the active area of the photodiode; A is the sensing area of the photodiode, and T is the transmittance of the tubing at 490 nm.

To account for the spatial distribution of light emission, Gaussian fitting is performed on the line profile of the mechanoluminescence emission, with the full width at half maximum (FWHM) used as the defining feature (**Supplementary Fig. 4c**). To estimate the peak power density of the FUS-induced light emission, a two-dimensional Gaussian function is employed to model the spatial distribution of the emission intensity (**Supplementary Fig. 4d**). The emission intensity as a function of radial distance r is defined in eq. (2):

$$I = I_0 exp(-\frac{r^2}{2\sigma^2}) \quad (2)$$

where I_0 represents the peak power density and σ is the standard deviation of the two-dimensional Gaussian function. Specifically, σ can be derived from the FWHM (i.e., 0.6 mm) of the line intensity profile using eq. (3):

$$\sigma = \frac{FWHM}{2\sqrt{2ln2}} \quad (3)$$

The parameters of the Gaussian model are optimized by fitting the measured spatial profile of the emission intensity, ensuring that the total integrated area under the curve matches the calculated P_{total} in eq. (1). Based on the fitting results, the peak optical power density (I_0) of the mechanoluminescence emission from the top surface of the tubing is estimated to be 196 $\mu W/mm^2$.

Based on the results above, the peak optical power density at a location surrounded by MLNT emitters was estimated to be 392 $\mu W/mm^2$, twice that of the configuration with emitters on only one side. This “surrounded” configuration is more representative of the *in vivo* scenario, where the dense cerebrovascular network delivers light from circulating MLNTs from all directions within the ultrasound focus, which typically encompasses multiple capillaries. This *in vivo* ultrasound-mediated light source, however, exhibits a time-dependent local power density due to the gradual clearance of circulating MLNTs from blood circulation. To this end, we determined the circulation half-life of systemically delivered MLNTs as approximately 26 min (**Supplementary Fig. 5**). Taking these dynamics into account, the peak *in vivo* optical power density was estimated to be 217 $\mu W/mm^2$, immediately following MLNT administration and FUS application.

This estimation suggests that the FUS-mediated light source provides sufficient optical output to support a broad range of light-based biological applications. For example, the light intensity generated by MLNTs under FUS within the first 4 min after systemic delivery remains above 200 $\mu W/mm^2$ under an ultrasound pressure of 2.3 MPa, sufficient for inducing spiking in neurons expressing the light-gated channelrhodopsin-2 (ChR2)[1] and activating photoswitchable proteins such as pdDronpa within its operational switching threshold[2]. In addition to these proteins that require relatively high light intensity, the FUS-mediated light source can provide prolonged photoactivation (>29 min) of ChR variants with higher light sensitivity after a single systemic injection of MLNTs. These ChR variants include ChR2(H134R), which was used in this study (**Fig. 7**, **Supplementary Figs. 17-19**), as well as other ChR variants such as CoChR, ChRger[3], and ultra-sensitive opsins including step-function opsins (SFOs) and SOUL[4,5].

Supplementary Figures

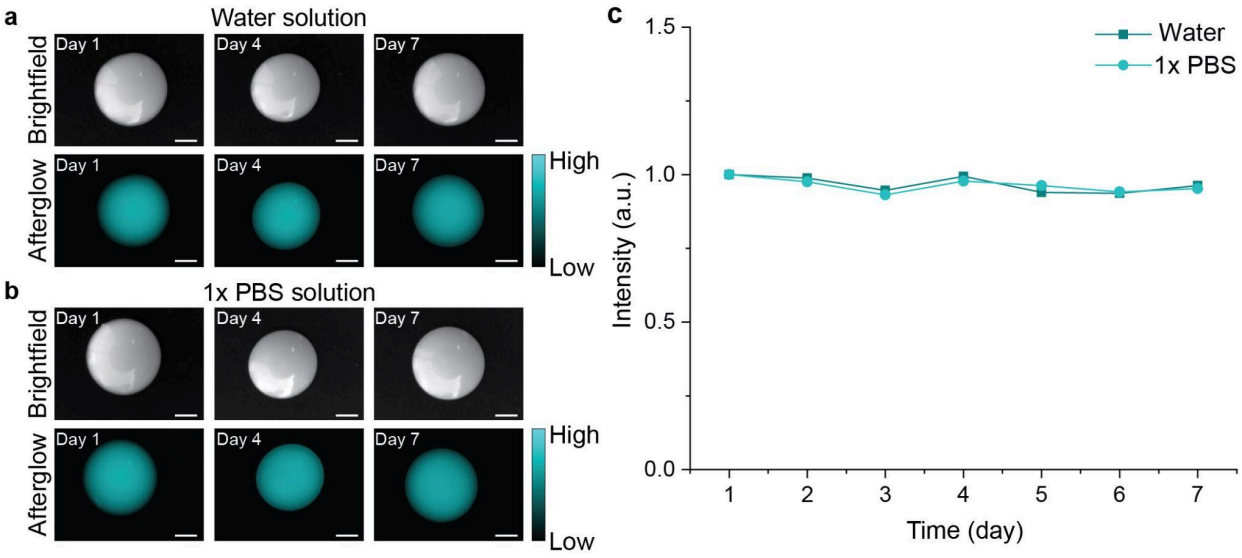

Supplementary Fig. 1. Stability assessment of MLNTs in water and 1x PBS. a-**b**, Brightfield (top) and afterglow (bottom) images of a 20 µL aliquot of MLNTs in water (**a**) and 1x PBS (**b**). Scale bars represent 2 mm. **c**, Afterglow intensity of MLNTs in water and 1x PBS over 7 days.

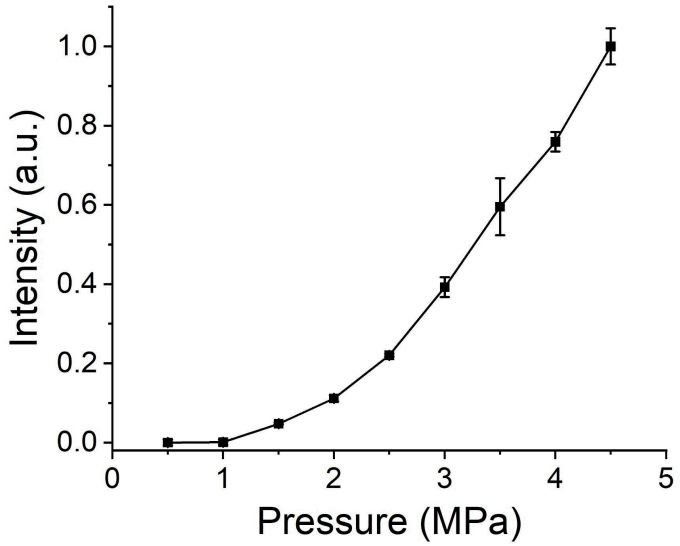

Supplementary Fig. 2. Dependence of the mechanoluminescence intensity of MLNTs on the pressure of applied FUS. All data are presented as mean ± s.d. from 3 measurements at each pressure value tested.

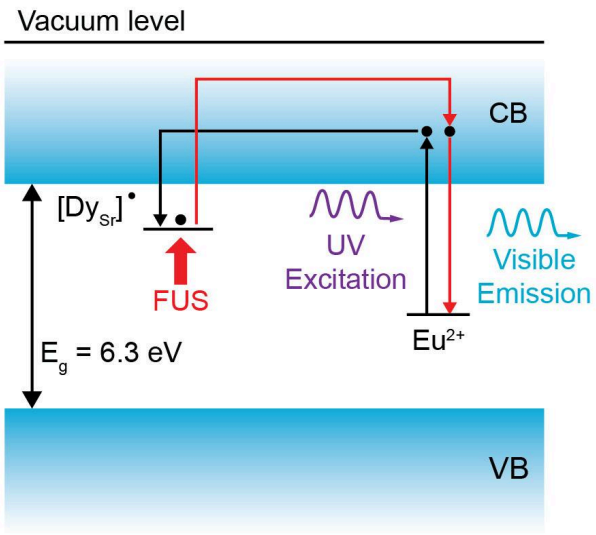

Supplementary Fig. 3. Schematic illustration of the mechanoluminescence mechanism in $Sr_4Al_{14}O_{25}$:Eu,Dy.

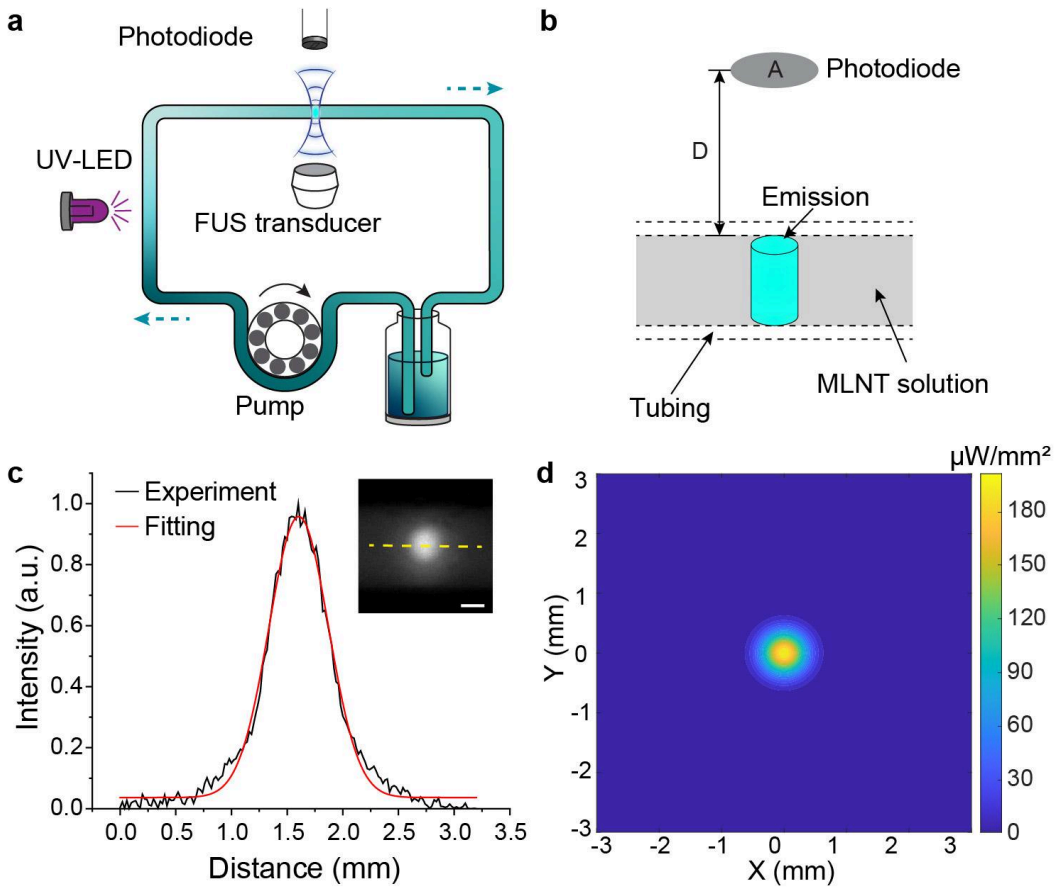

Supplementary Fig. 4. Optical power measurements of FUS-induced mechanoluminescence emission from MLNT solution in the artificial circulatory system. **a**, A schematic illustration of the experimental setup measuring the optical power during FUS pulses. **b**, A simplified schematic illustration of mechanoluminescence emission as a cylindrical source at the ultrasound focus. **c**, Line intensity profile along the yellow dashed line shown in the mechanoluminescence image in the inset. The scale bar represents 500 μm in the inset. **d**, A two-dimensional plot of the Gaussian power distribution as a projection onto the xy plane, with the colorbar indicating the power density of light emission from the upper surface of the cylindrical light source.

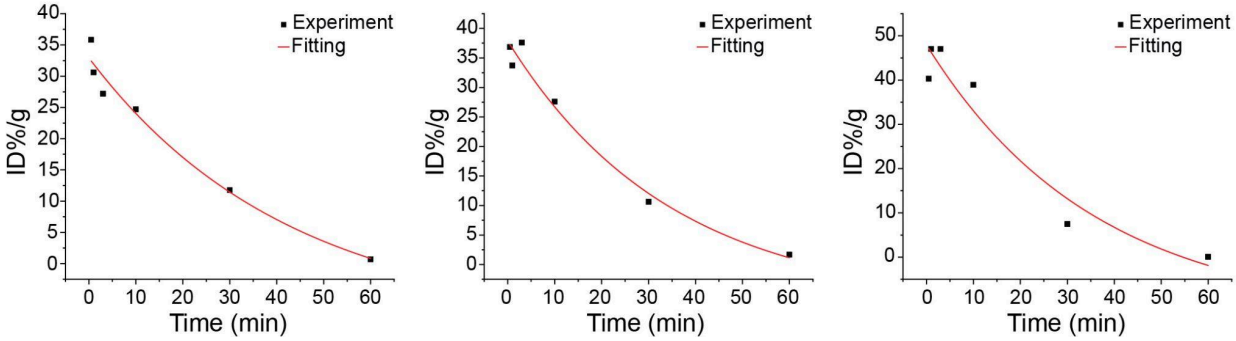

Supplementary Fig. 5. Concentration measurements of MLNTs in the mouse's bloodstream. Three independent measurements of the MLNT concentrations in the blood samples, which were collected 30 s, 1 min, 3 min, 10 min, 30 min, and 60 min after systemic administration. The black dots represent the experimental data, while the red curve corresponds to first-order exponential decay fitting. ID%/g represents percentage of injected dose per gram of tissue (in this case, blood).

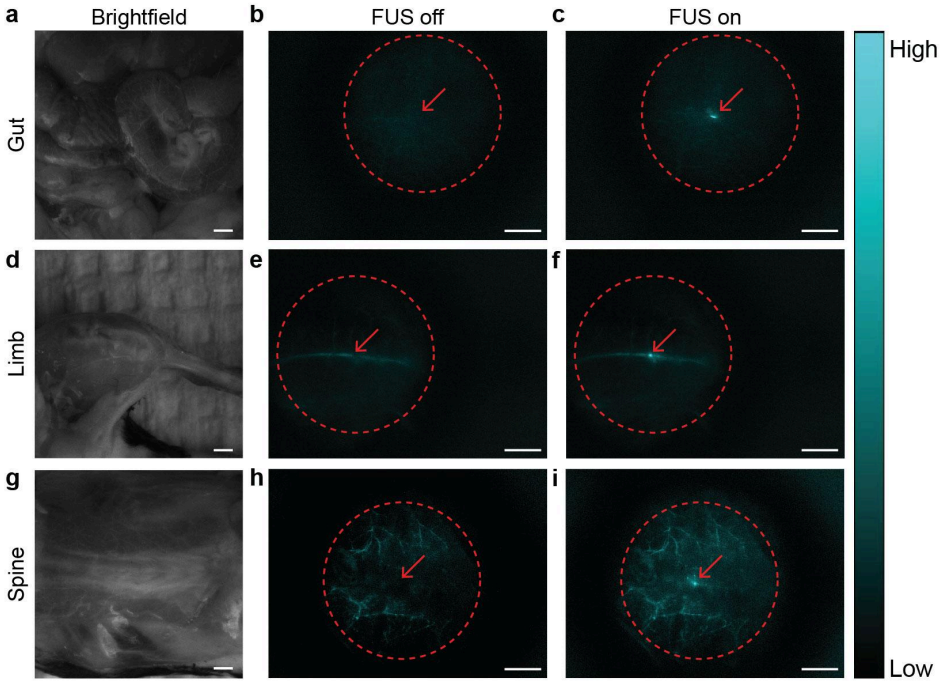

Supplementary Fig. 6. Mechanoluminescence emission from peripheral organs. a, d, g, Brightfield images of the gut (**a**), limb (**d**), and spine (**g**). **b-c, e-f, h-i**, Luminescence images of the mouse gut (**b-c**), limb (**e-f**), and spine (**h-i**) before (**b, e, h**) and after (**c, f, i**) the application of FUS. Dashed red circles indicate the imaging region through the ring transducer, while red arrows highlight the focus of ultrasound. Scale bars represent 2 mm.

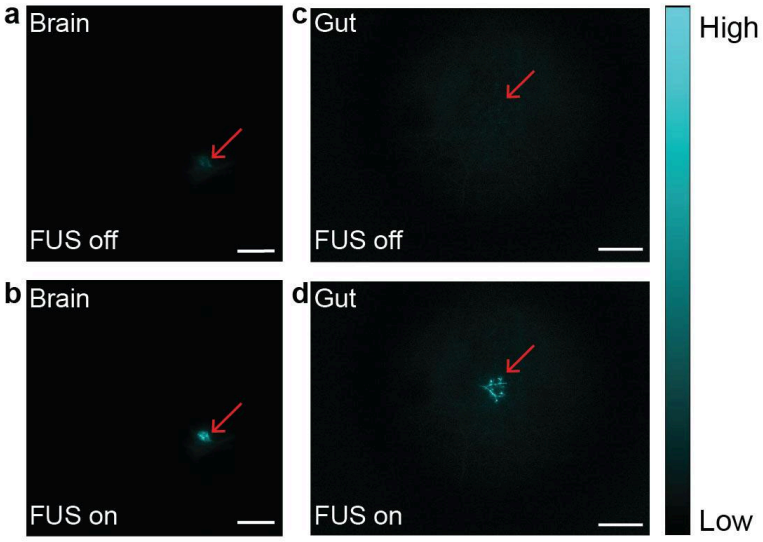

Supplementary Fig. 7. Mechanoluminescence emissions from multiple vessels within the ultrasound focus. a-b, A representative image taken in the brain when FUS was off (**a**) and on (**b**). **c-d**, A representative image taken in the gut when the FUS was off (**c**) and on (**d**). The red arrows highlight the ultrasound focus. Scale bars represent 2 mm.

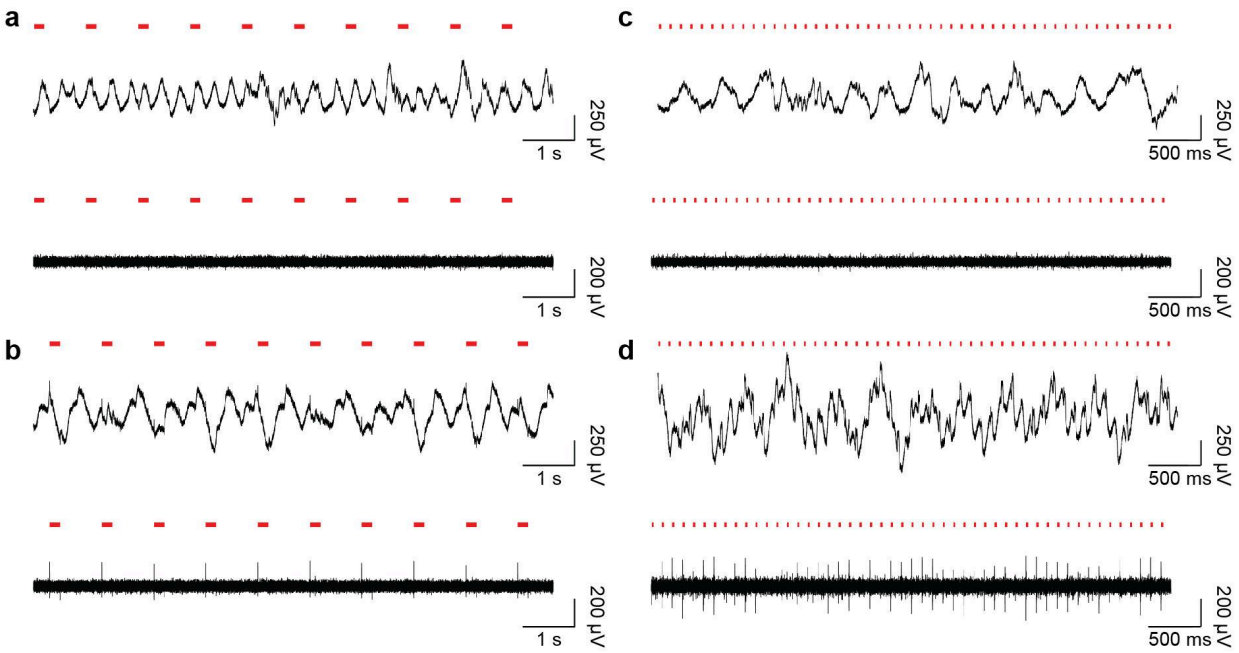

Supplementary Fig. 8. Raw and filtered electrophysiological recordings in the mouse brain under different experimental conditions. a-**b**, Electrophysiological recordings under 1 Hz FUS pulses without (**a**) and with (**b**) circulating MLNTs. **c**-**d**, Electrophysiological recordings under 10 Hz FUS pulses without (**c**) and with (**d**) circulating MLNTs. Red ticks indicate the duration of FUS pulses. In each panel, the top trace presents the unfiltered raw data while the bottom trace represents bandpass-filtered (0.25−6 kHz) spiking activities.

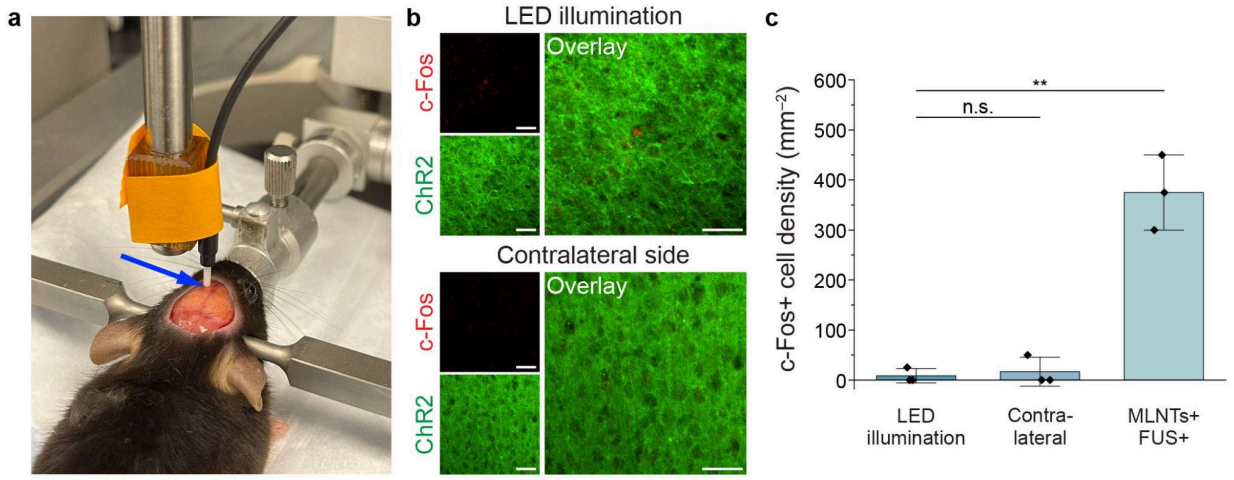

Supplementary Fig. 9. LED cannot stimulate M1 neurons through the skull. a, A photograph of the experimental setup. The blue arrow indicates the optical fiber positioned immediately above the exposed skull overlying the M1 region. **b**, Representative immunostaining images from the M1 region illuminated by the LED through the skull and the corresponding region in the contralateral hemisphere. **c**, Statistical analysis of the c-Fos cell density under different conditions. The MLNTs+/FUS+ condition represents another group of mice receiving systemic injection of MLNTs and FUS stimulation in the M1 region. One-way ANOVA, LED illumination vs contralateral side: $F_{(1,\ 4)}$=0.2, P=0.68; LED illumination vs MLNTs(+)/FUS(+): $F_{(1,\ 4)}$=69.14, P=0.0011. Scale bars represent 40 μm. All data are presented as mean ± s.d. with data points shown for each animal from n = 3 mice in each group. $P \geq 0.05$ (n.s.), $^{**}P < 0.01$.

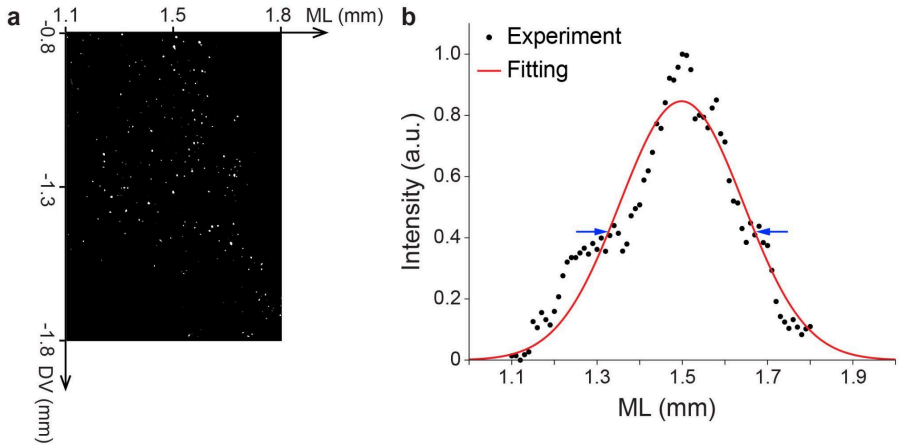

Supplementary Fig. 10. Estimation of brain tissue volume activated by the ultrasound-scanning *in vivo* light source based on immunostaining of c-Fos. a, A representative coronal brain section from a mouse with circulating MLNTs, showing the region where FUS was applied. c-Fos positive neurons are indicated by white dots. **b**, Gaussian fit of the c-Fos intensity profile, which was projected onto the ML axis, yields an estimated FWHM of 341 μm.

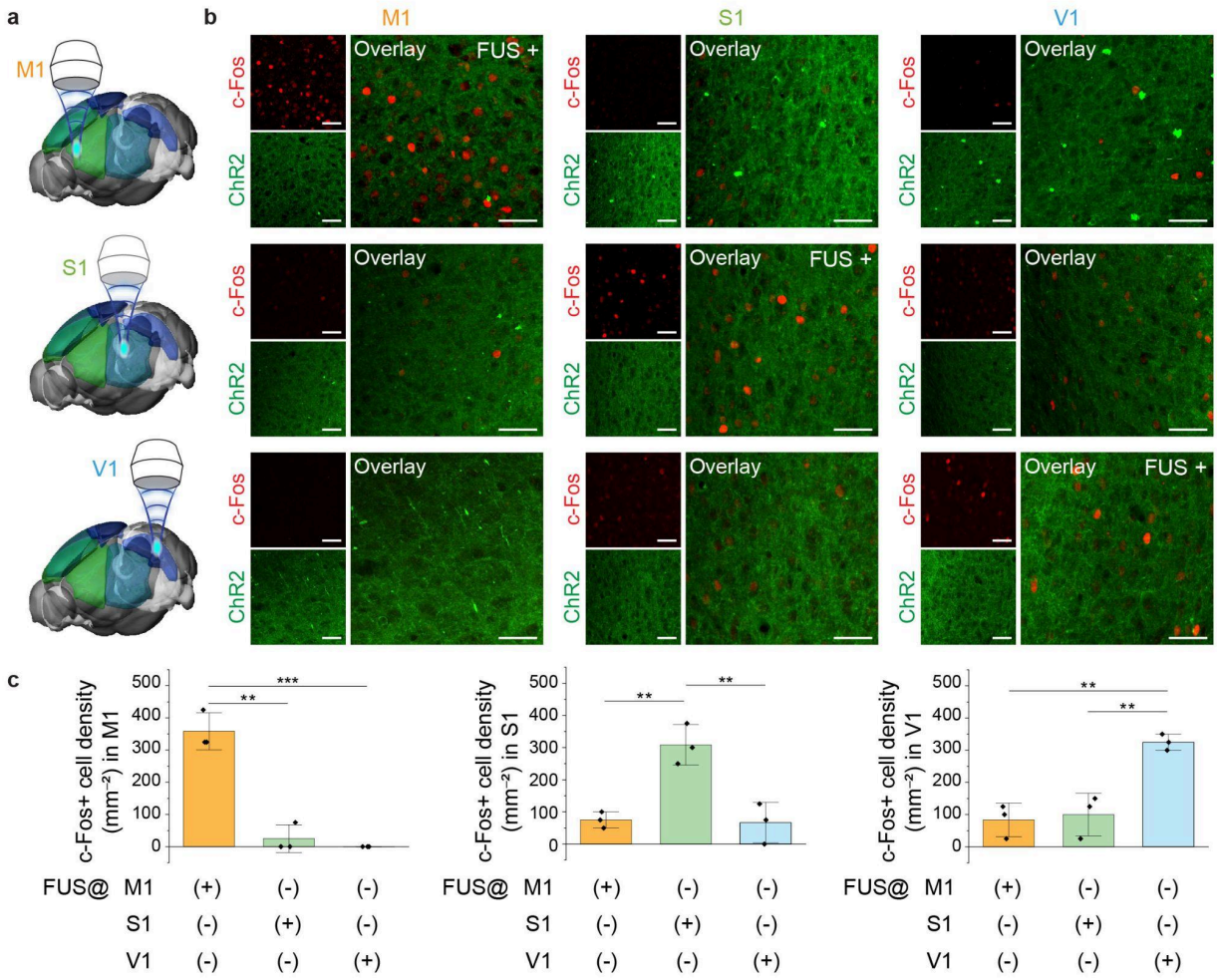

Supplementary Fig. 11. Validation of c-Fos expression across different brain regions following region-specific light emission by FUS. **a**, Schematic illustration of the FUS-mediated light source applied to individual brain regions: M1 (top), S1 (middle), and the primary visual cortex (V1, bottom). **b**, Representative immunostaining images of ChR2 and c-Fos in M1, S1, and V1 regions when FUS is only applied to one of these regions at a time. **c**, Statistical analysis of the c-Fos cell density under different experimental conditions. One-way ANOVA, c-Fos in the M1 region: FUS@M1 vs FUS@S1: $F_{(1,\ 4)}$=64, P=0.0013; FUS@M1 vs FUS@V1: $F_{(1,\ 4)}$=115.56, P=0.00042. c-Fos in the S1 region, FUS@S1 vs FUS@M1: $F_{(1,\ 4)}$=35.64, P=0.0040; FUS@S1 vs FUS@V1: $F_{(1,\ 4)}$=22.13, P=0.0093. c-Fos in the V1 region, FUS@V1 vs FUS@M1: $F_{(1,\ 4)}$=52.56, P=0.0019; FUS@V1 vs FUS@S1: $F_{(1,\ 4)}$=30.38, P=0.0053. All data are presented as mean ± s.d. with data points shown for each animal from n = 3 mice in each group. Scale bars represent 40 μm. $^{**}P < 0.01$, $^{***}P < 0.001$.

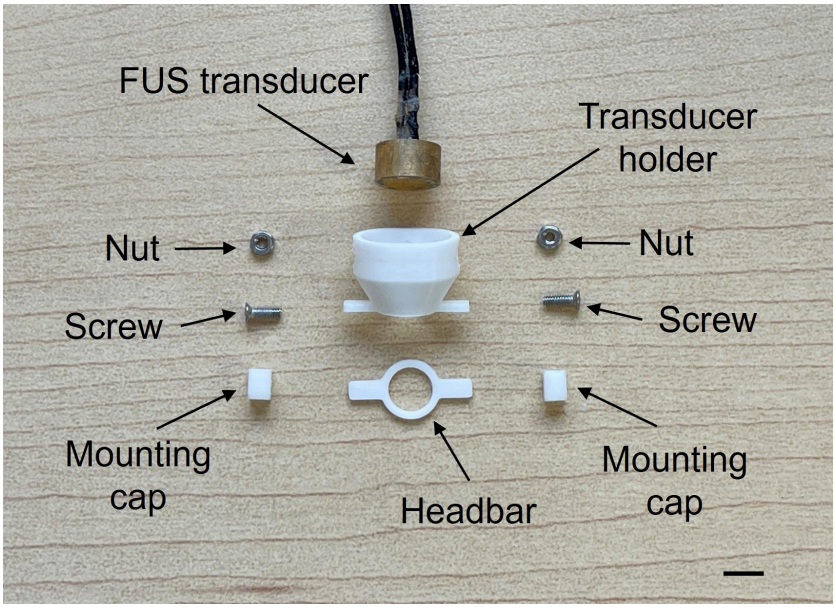

Supplementary Fig. 12. A photograph of the components for the head-mounting system, including the FUS transducer, transducer holder, headbar, mounting caps, focus-adjusting screws, and nuts. The scale bar represents 5 mm.

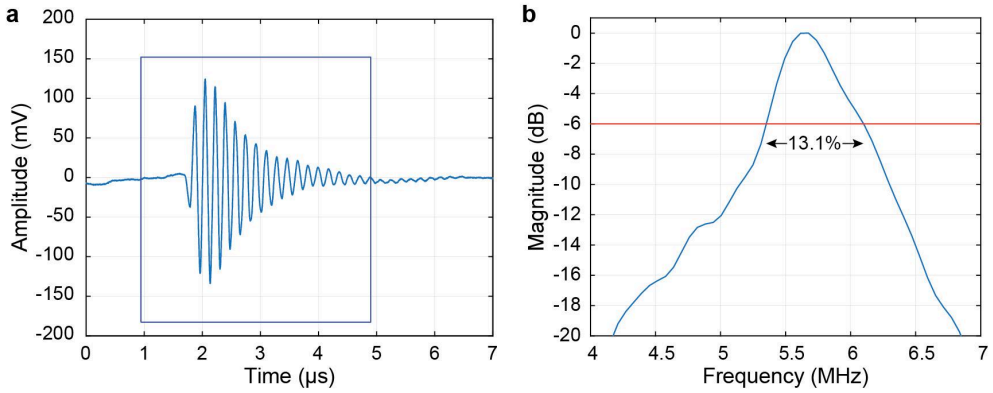

Supplementary Fig. 13. Characterizations of the wearable transducer. (**a**) Pulse-echo response of the 5.7 MHz wearable transducer. (**b**) The fast Fourier transform (FFT) spectrum of the pulse-echo signal highlighted by the blue box in (**a**), showing the central frequency of 5.7 MHz and -6 dB fractional bandwidth of 13.1%.

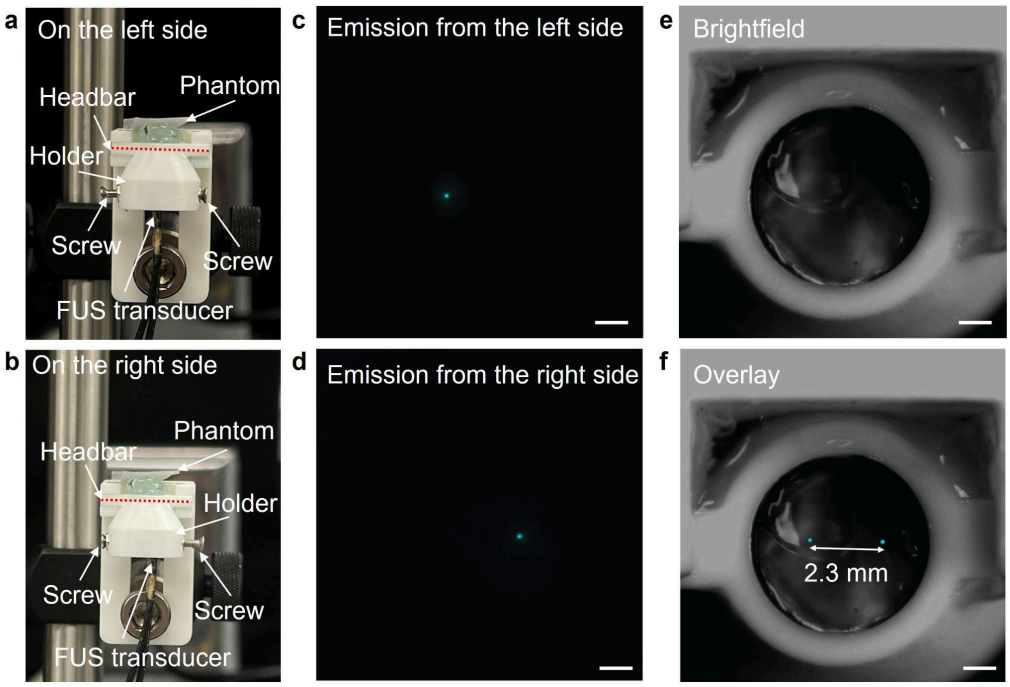

Supplementary Fig. 14. Mechanoluminescence emission produced by the wearable transducer with adjustable focus. a-**b**, Side-view photographs of the experimental setup where the ultrasound is focused on the left (**a**) or the right (**b**) side of the transducer holder. **c**-**d**, Representative mechanoluminescence images under ultrasound with its focus on the left (**c**) or the right (**d**) side. **e**, Top-view brightfield image of the headbar. **f**, Overlay of mechanoluminescence (cyan) from **c**-**d** and the brightfield image from **e**, showing distinct mechanoluminescence emission spots separated by 2.3 mm. Scale bars represent 1 mm.

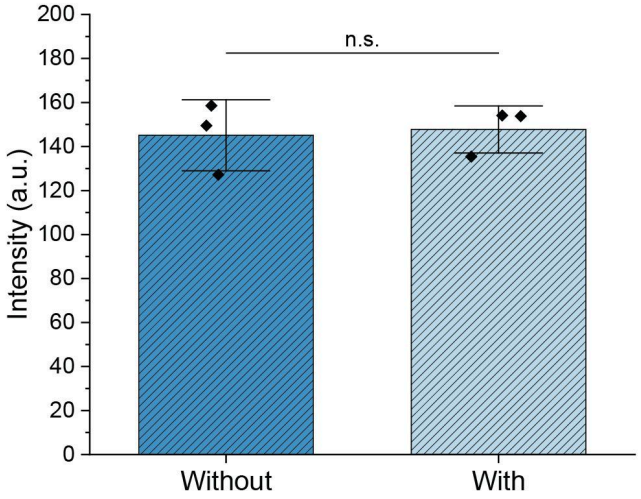

Supplementary Fig. 15. Mechanoluminescence with or without the commutator. One-way ANOVA, $F_{(1, 4)}$=0.06, P=0.82. All data are presented as mean ± s.d. with data points shown for 3 measurements in each group. $P \geq 0.05$ (n.s.).

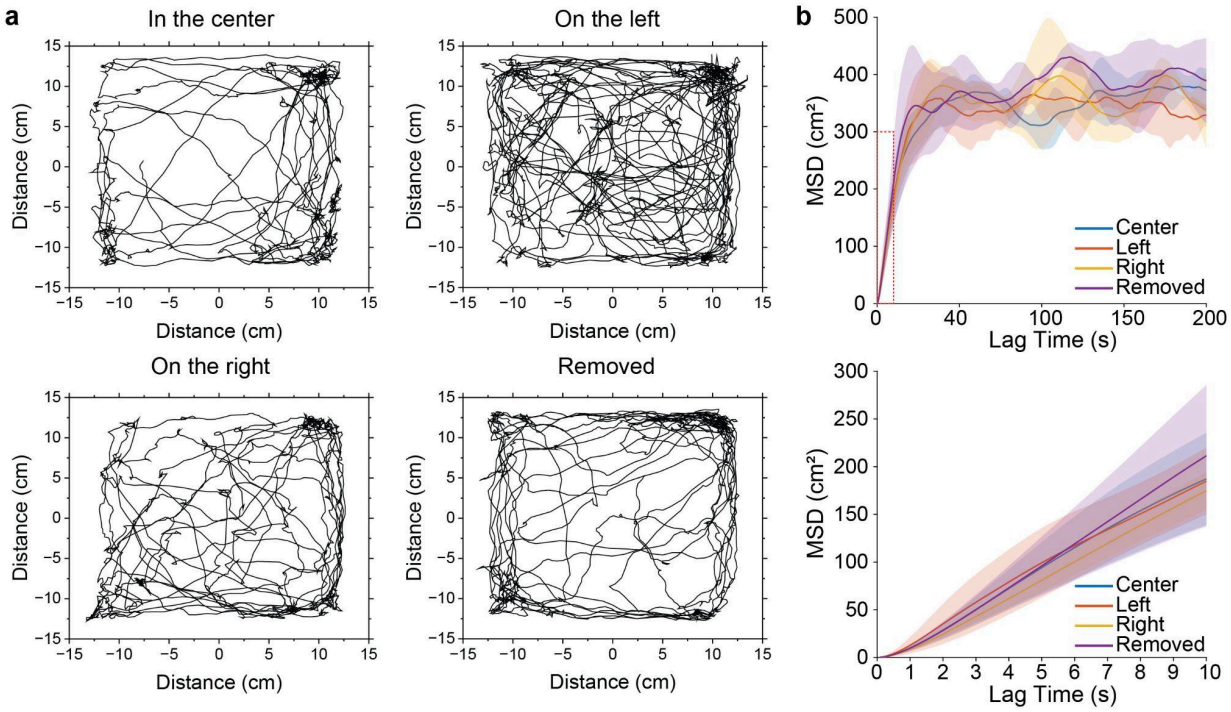

Supplementary Fig. 16. Mouse movement under varying transducer positions. **a**, Representative trajectories of a mouse with the transducer positioned in the center, on the left, on the right, or removed. **b**, Mean squared displacement (MSD) analysis of the animal with the transducer at different locations: center (blue), left (red), right (yellow), and removed (purple). The top plot shows the lag time up to 200 s and the bottom plot represents the zoomed view of 0-10 s from the red box in the top graph. Data are presented as mean (solid lines) ± s.d. (shaded area) from n = 3 mice at each transduction configuration.

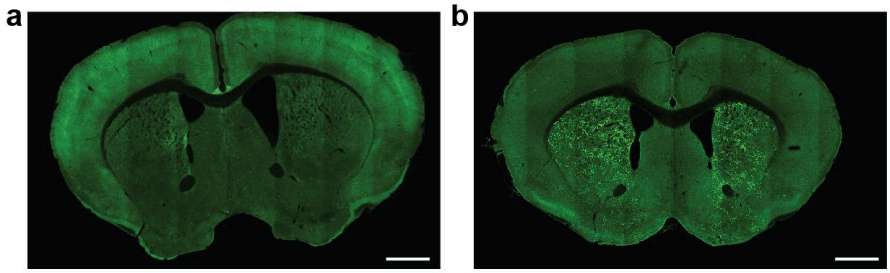

Supplementary Fig. 17. Validation of ChR2 expression in the brains of D1-Cre and A2a-Cre mice following systemic injection of AAV-PHP.eB-EF1a-double floxed-hChR2(H134R)-EYFP-WPRE-HGHpA. Representative confocal images of coronal brain sections from a D1-Cre mouse (**a**) and an A2a-Cre mouse (**b**). Scale bars represent 1 mm.

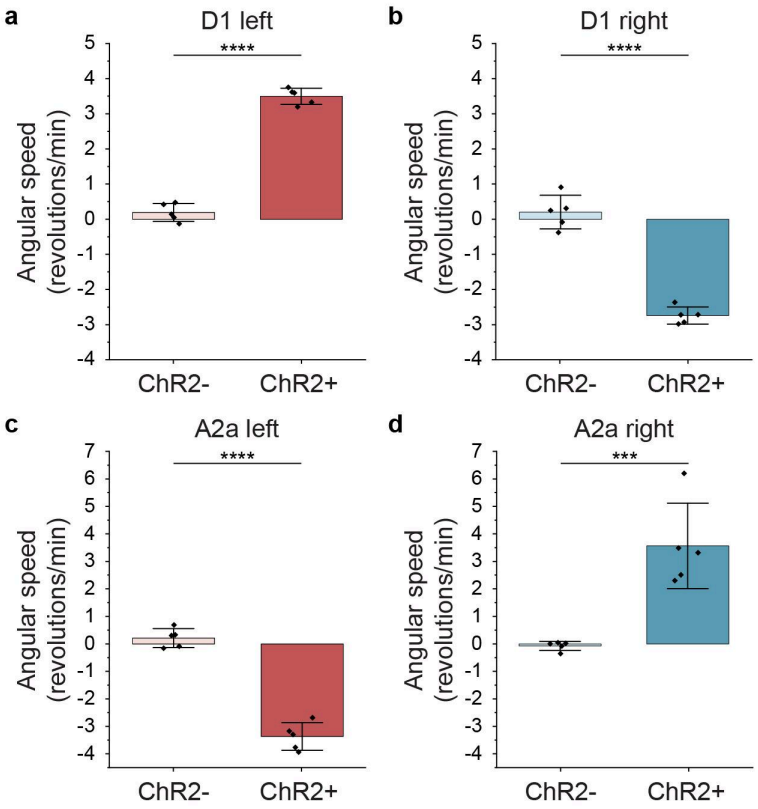

Supplementary Fig. 18. Angular displacements from different animals under varying conditions. **a-b**, Statistical analysis of angular displacements from D1-YFP (i.e., ChR2-) and D1-ChR2-YFP (i.e., ChR2+) mice when FUS was applied to target striatal regions in left (**a**) and right (**b**) hemispheres. **c-d**, Statistical analysis of angular displacements from A2a-YFP (i.e., ChR2-) and A2a-ChR2-YFP (i.e., ChR2+) mice when FUS was applied to target striatal regions in left (**c**) and right (**d**) hemispheres. All animals received systemic administration of MLNTs before FUS stimulation (see Methods). One-way ANOVA, D1 left: $F_{(1,\ 8)}$=468.25, $P < 0.0001$; D1 right: $F_{(1,\ 8)}$=149.22, $P < 0.0001$; A2a left: $F_{(1,\ 8)}$=175.60, $P < 0.0001$; A2a right: $F_{(1,\ 8)}$=26.90, P=0.00084. All data are presented as mean ± s.d. with data points shown for each animal from n = 5 mice in each group. ***$P < 0.001$, ****$P < 0.0001$.

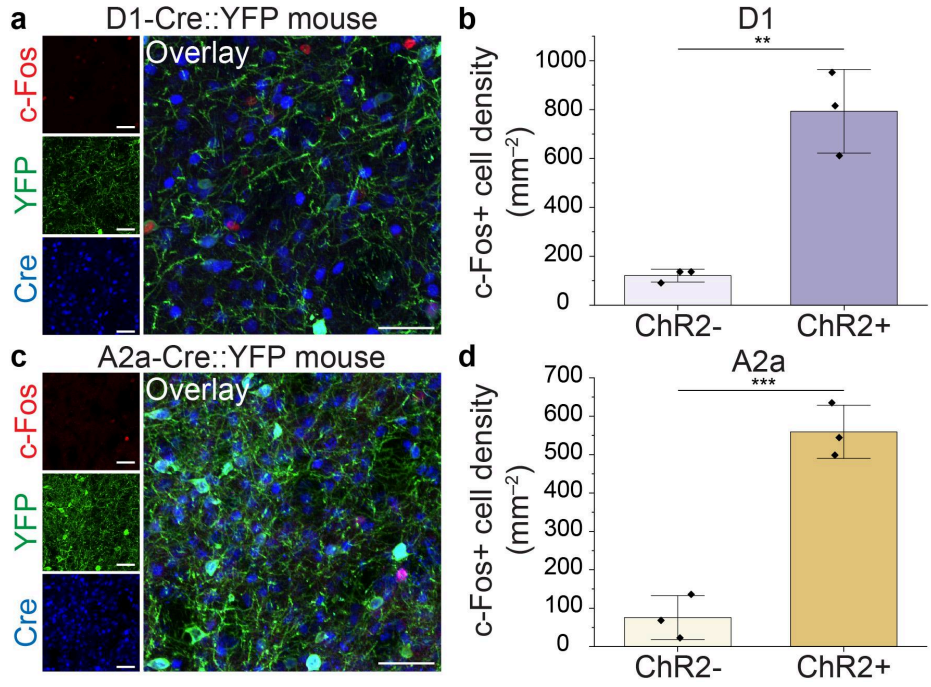

Supplementary Fig. 19. c-Fos expression of D1- or A2a-Cre::YFP mice after being stimulated by the ultrasound-scanning *in vivo* light source. a, c, Representative confocal images of the left striatum region of D1-Cre::YFP mice (**a**) and A2a-Cre::YFP mice (**c**) after FUS-mediated photostimulation. **b**, Statistical analysis of c-Fos cell density for D1-Cre::YFP mice and D1-Cre::ChR2-YFP mice after FUS-mediated photostimulation in the left striatum. **d**, Statistical analysis of c-Fos cell density for A2a-Cre::YFP mice and A2a-Cre::ChR2-YFP mice after FUS-mediated photostimulation in the left striatum. One-way ANOVA, D1: $F_{(1,\ 4)}$=45.26, P=0.0025; A2a: $F_{(1,\ 4)}$=87.15, P=0.00073. Scale bars represent 40 μm. All data are presented as mean ± s.d. with data points shown for each animal from n = 3 mice in each group. $^{**}P < 0.01$, $^{***}P < 0.001$.

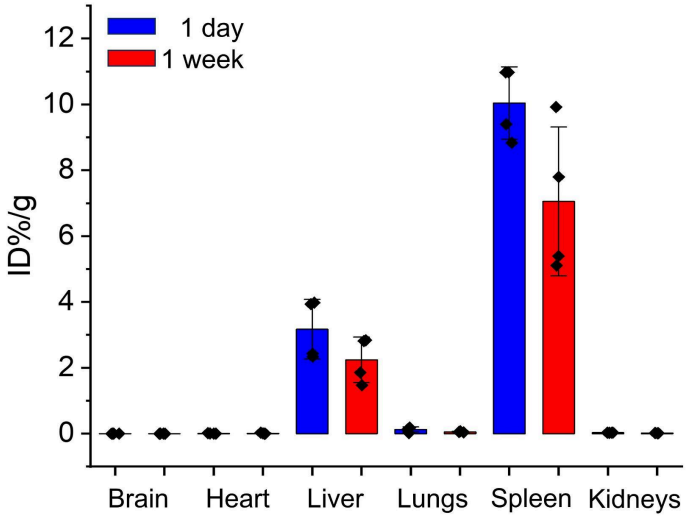

Supplementary Fig. 20. Biodistribution of systemically delivered MLNTs (200 µL of 30 mg/ml) in major organs at one day (blue) and one week (red) post-injection. All data are presented as mean ± s.d. with data points shown for each animal from n = 4 mice in each group.

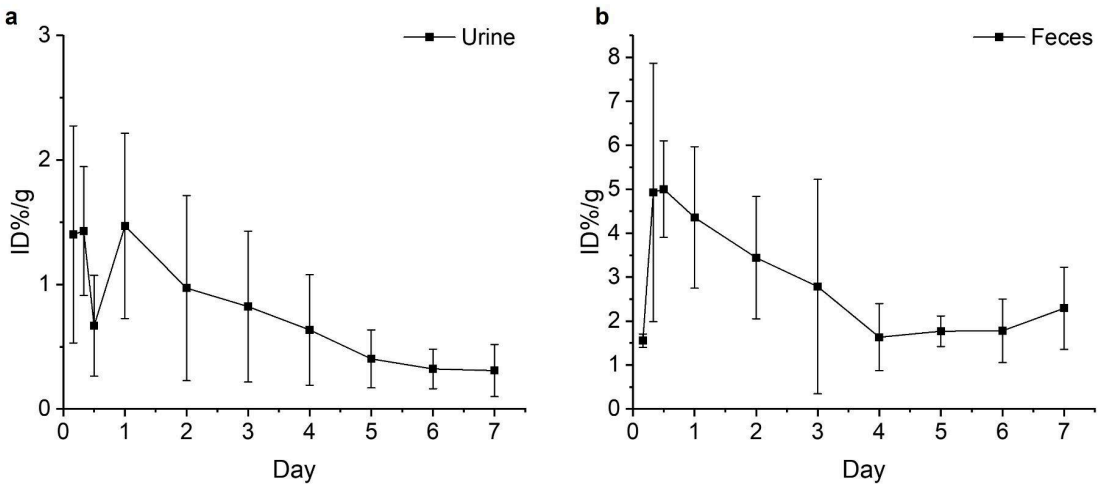

Supplementary Fig. 21. *In vivo* clearance study of intravenously administered MLNTs. **a**-**b**, Excretion profiles of MLNTs in the urine (**a**) and feces (**b**) after intravenous injection of MLNTs. All data are presented as mean ± s.d. with data points shown for each animal from n = 4 mice in each group.

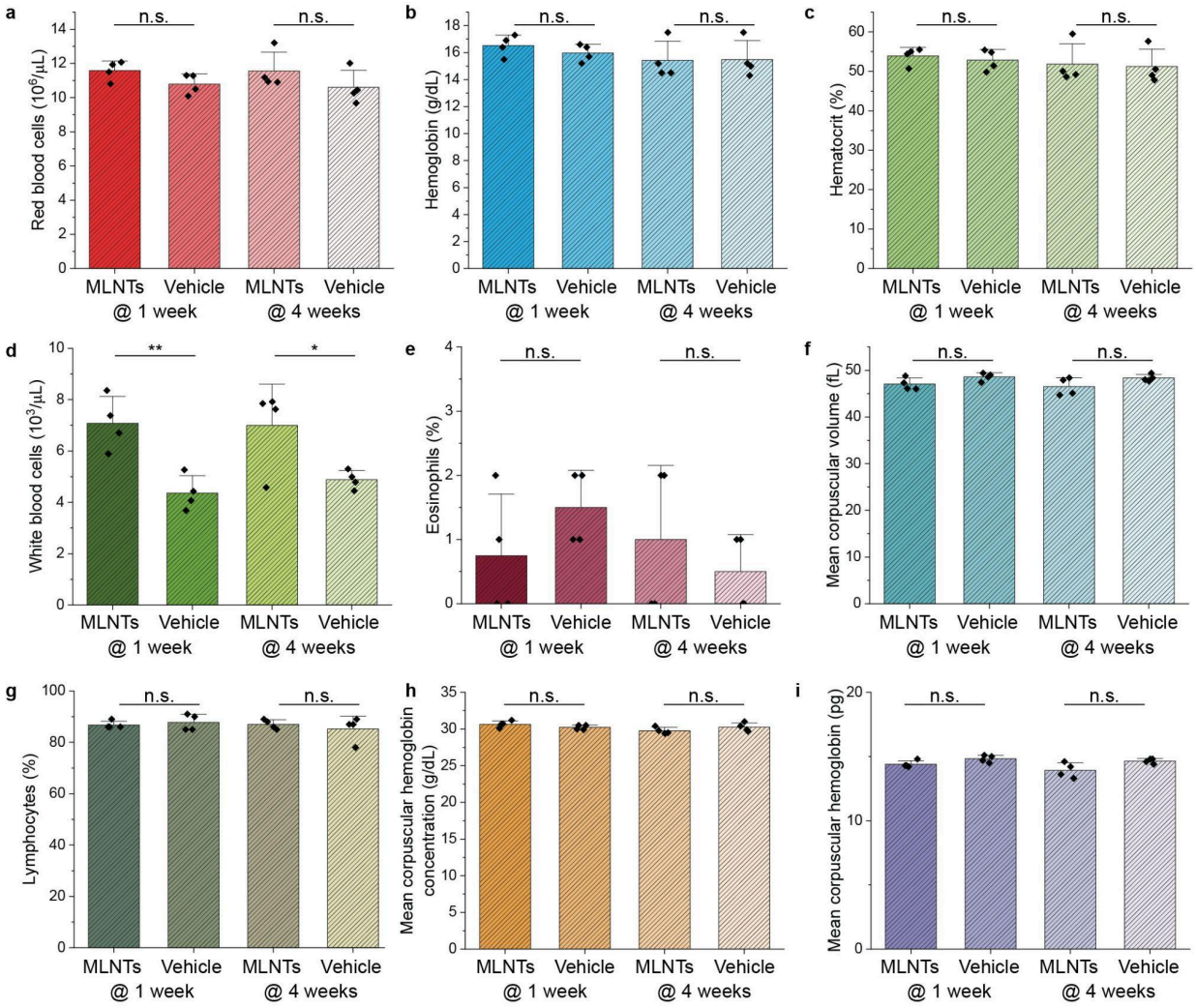

Supplementary Fig. 22. Complete blood count (CBC) tests. CBC results of mice are shown for 1 week and 4 weeks after intravenous injection of MLNTs in 1x PBS solution or vehicle (i.e., 1x PBS without MLNTs). The test results include red blood cells (**a**), hemoglobin (**b**), hematocrit (**c**), white blood cells (**d**), eosinophils (**e**), mean corpuscular volume (**f**), lymphocytes (**g**), mean corpuscular hemoglobin concentration (**h**), and mean corpuscular hemoglobin (**i**). All data are presented as mean + s.d. with data points shown for each animal from n = 4 mice in each group. One-way ANOVA, red blood cells, 1 week: $F_{(1, 6)}$=3.63, P=0.11; 4 weeks: $F_{(1, 6)}$=1.64, P=0.25. Hemoglobin, 1 week: $F_{(1, 6)}$=1.19, P=0.32; 4 weeks: $F_{(1, 6)}$=0.0057, P=0.94. Hematocrit, 1 week: $F_{(1, 6)}$=0.37, P=0.57; 4 weeks: $F_{(1, 6)}$=0.03, P=0.87. White blood cells, 1 week: $F_{(1, 6)}$=19.02, P=0.0048; 4 weeks: $F_{(1, 6)}$=6.23, P=0.043. Eosinophils, 1 week: $F_{(1, 6)}$=1.8, P=0.23; 4 weeks: $F_{(1, 6)}$=0.6, P=0.47. Mean corpuscular volume, 1 week: $F_{(1, 6)}$=3.91, P=0.095; 4 weeks: $F_{(1, 6)}$=3.31, P=0.12. Lymphocytes, 1 week: $F_{(1, 6)}$=0.32, P=0.59; 4 weeks: $F_{(1, 6)}$=0.31, P=0.60. Mean corpuscular hemoglobin concentration, 1 week: $F_{(1, 6)}$=2.36, P=0.18; 4 weeks: $F_{(1, 6)}$=1.67, P=0.24. Mean corpuscular hemoglobin, 1 week: $F_{(1, 6)}$=4.84, P=0.070; 4 weeks: $F_{(1, 6)}$=5.55, P=0.057. $P \geq 0.05$ (n.s.), *$P < 0.05$, **$P < 0.01$.

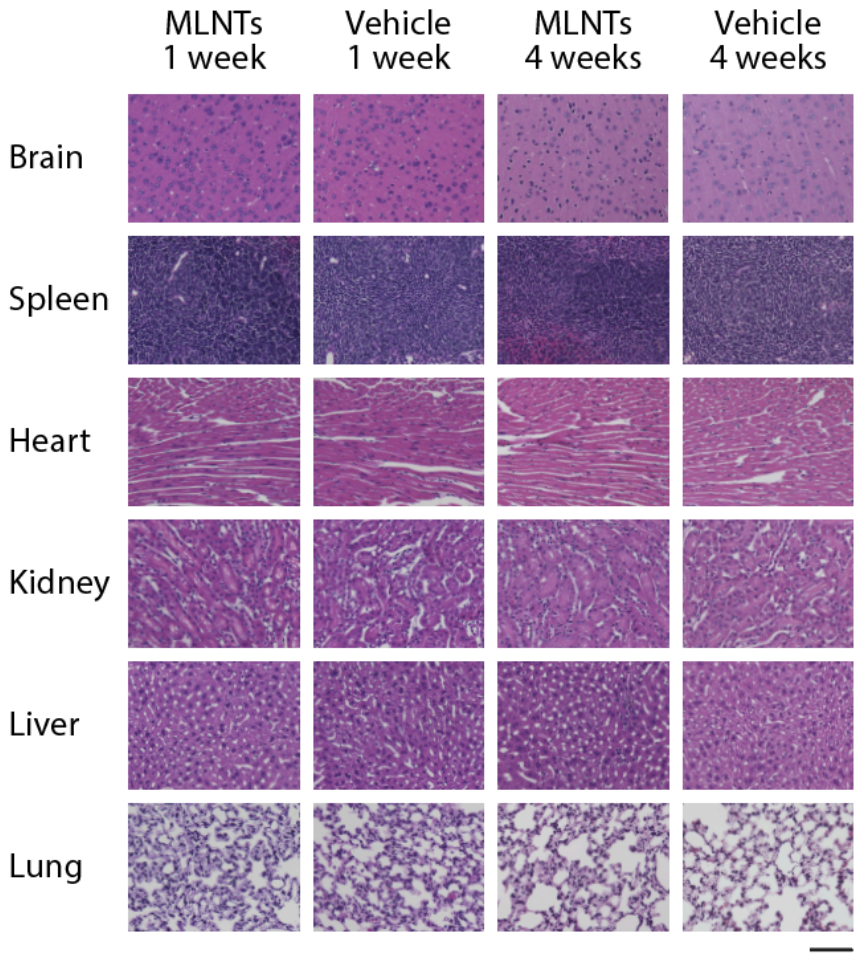

Supplementary Fig. 23. Histopathological analysis of mouse organs. Representative Hematoxylin and eosin (H&E) stained images of the brain, spleen, heart, kidney, liver, and lung from mice 1 and 4 weeks after intravenous injection of MLNT solution (200 μL, 30 mg/mL) or vehicle control (200 μL, 1× PBS), n = 4 for each group. No noticeable pathological differences were observed among all groups. The scale bar represents 100 μm.

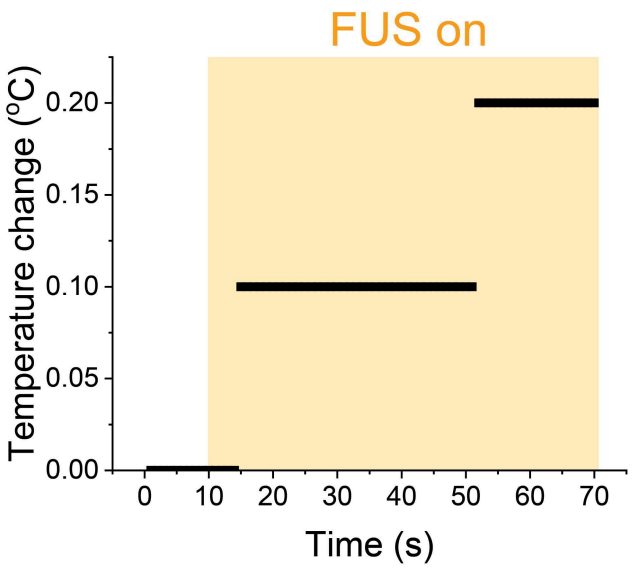

Supplementary Fig. 24. *In vivo* brain temperature monitoring during FUS stimulation. Representative trace showing the recorded brain temperature *in vivo* during FUS stimulation applied at 1 Hz with a 20% duty cycle. FUS was started at 10 s, as indicated by the yellow shaded region. The recorded temperature is highly discretized due to the limited resolution of the thermal probe (0.1 ℃).

Supplementary Table 1. Antibodies used in this study.

Primary antibodies	Secondary antibodies
Rabbit anti-c-Fos (1:500, ab222699, abcam)	Donkey anti-rabbit, Alexa Fluor 594 (1:500, A-21207, Invitrogen)
	Goat anti-rabbit, Cyanine Cy3 (1:500, 111-165-144, Jackson ImmunoResearch)
Chicken anti-green fluorescent protein (1:500, GFP-1010, aveslabs)	Goat anti-chicken, Alexa Fluor 488 (1:500, 103-545-155, Jackson ImmunoResearch)
Guinea pig anti-cre recombinase (1:500, 257005, Synaptic Systems)	Goat anti-guinea pig, Alexa Fluor 647 (1:500, 106-605-003, Jackson ImmunoResearch)
Guinea pig anti-NeuN (1:500, 266004, Synaptic Systems)	Goat anti-guinea pig, Alexa Fluor 647 (1:500, 106-605-003, Jackson ImmunoResearch)
Chicken anti-GFAP (1:500, ab4674, abcam)	Goat anti-chicken, Alexa Fluor 488 (1:500, 103-545-155, Jackson ImmunoResearch)
Rabbit anti-Iba1 (1:500, 019-19741, Wako Chemicals)	Goat anti-rabbit, Cyanine Cy3 (1:500, 111-165-144, Jackson ImmunoResearch)

Supplementary Movie 1. Dynamic ultrasound-mediated photostimulation of the left striatum on freely moving D1-Cre::ChR2-YFP mouse.
The FUS-scanning light source first induced counter-clockwise circling (viewed from below) in a freely moving D1-Cre::ChR2-YFP mouse during left striatal stimulation. The movie is played at 3× speed.

Supplementary Movie 2. Dynamic ultrasound-mediated photostimulation of the right striatum on freely moving D1-Cre::ChR2-YFP mouse.
Subsequently, the same D1-Cre::ChR2-YFP mouse as shown in Supplementary Movie 1 exhibited clockwise circling (viewed from below) when the ultrasound focus was adjusted to target the right striatum. The movie is played at 3× speed.

Supplementary Movie 3. Dynamic ultrasound-mediated photostimulation of the left striatum on freely moving A2a-Cre::ChR2-YFP mouse.
The FUS-scanning light source first induced clockwise circling (viewed from below) in a freely moving A2a-Cre::ChR2-YFP mouse during left striatal stimulation. The movie is played at 3× speed.

Supplementary Movie 4. Dynamic ultrasound-mediated photostimulation of the right striatum on freely moving A2a-Cre::ChR2-YFP mouse.
Subsequently, the same A2a-Cre::ChR2-YFP mouse as shown in Supplementary Movie 3 exhibited counter-clockwise circling (viewed from below) when the ultrasound focus was adjusted to target the right striatum. The movie is played at 3× speed.

References

1. Klapoetke, N. C. *et al.* Independent optical excitation of distinct neural populations. *Nat. Methods* **11**, 338–346 (2014).
2. Zhou, X. X., Fan, L. Z., Li, P., Shen, K. & Lin, M. Z. Optical control of cell signaling by single-chain photoswitchable kinases. *Science* **355**, 836–842 (2017).
3. Bedbrook, C. N. *et al.* Machine learning-guided channelrhodopsin engineering enables minimally invasive optogenetics. *Nat. Methods* **16**, 1176–1184 (2019).
4. Gong, X. *et al.* An ultra-sensitive step-function opsin for minimally invasive optogenetic stimulation in mice and macaques. *Neuron* **107**, 38–51.e8 (2020).
5. Yizhar, O. *et al.* Neocortical excitation/inhibition balance in information processing and social dysfunction. *Nature* **477**, 171–178 (2011).